이학석사 학위논문

Sorting of human mesenchymal stem cells by applying microfluidic chip filtration combined with inertial focusing

관성 집중을 수반하는 미세유체칩 여과에 의한 인간 중간엽 줄기세포의 크기별 분리 분석

2017 년 8 월

서울대학교 대학원

치의과학과 구강악안면 해부 및 영상과학 전공

심 창 재

관성 집중을 수반하는 미세유체칩 여과에 의한 인간 중간엽 줄기세포의 크기별 분리 분석

지도교수 장 미 숙

이 논문을 이학석사학위 논문으로 제출함

2017년 4월

서울대학교 대학원

치의과학과 구강악안면 해부 및 영상과학 전공

심 창 재

심창재의 이학석사학위 논문을 인준함

2017년 6월

위 원 장 홍승훈 (인)

부 위 원 장 장 미 숙 (인)

위 원 전명석 (인)

Abstract

Sorting of human mesenchymal stem cells by applying microfluidic chip filtration combined with inertial focusing

Chang Jae Shim

Department of Oral Anatomy

The Graduate School

Seoul National University

(Directed by Prof. Mi-Sook Chang, D.D.S., Ph.D.)

Human bone marrow-derived mesenchymal stem cells (hMSCs) are promising cell sources for stem cell therapy because of their low immunogenicity, multipotency and self-renewal capacity. In the recent study, it has been reported that hMSCs consist of heterogeneous subpopulations: rapidly self-renewing (RS) cells, spindle-shaped (SS) cells, and flattened and large (FL) cells. Furthermore, RS and SS subpopulations of hMCSs show

higher multipotent capacities than cells in the FL group. Because each subpopulation has different proliferative and multipotent capacities, sorting out a specific subpopulation of cells from total cell population is a significant approach for stem cell researches including cell therapy.

In this study, to improve separation efficiency, a channel design combining inertial focusing with microfluidic chip filtration was attempted and applied to the size-dependent separation of hMSCs. The channel networks were designed based on the precise calculations of a model for the fluid flow and cut-off width of the hMSCs to be separated. Polydimethylsiloxane (PDMS)-glass chip was fabricated by means of microelectromechanical system (MEMS) process, and the chip had a main channel for the input of an hMSC suspension, a side channel for cell-free media focusing of cells to the opposite sidewall and several multi-branched channels. Multi-branched channels converged on a seven-turn spiral channel where the hMSCs were focused on certain equilibrium positions. Focused hMSCs can be collected from the outlets by size. In addition, the end of the main channel was converted into a spiral channel where the hMSCs experienced further focusing and exited through the outlets. Eventually, the efficiencies of cell separation were 83% and 98% for the small

cells (RS and SS) with high differentiation potential and the large cell (FL) group with low differentiation potential for recovery, respectively. The purities were confirmed to be 99% and 76%, respectively. These result showed higher efficiency and throughput than the result of previous microfluidic chip filtration. Thus, size-dependent sorting of hMSCs by microfluidic chip filtration combined with inertial focusing is expected to hold promise for stem cell research.

Keywords: Human mesenchymal stem cell, Size-dependent separation, Inertial focusing, Microfluidic chip filtration, Channel design

Student Number: 2015-22089

Contents

Chapter

List of figures

List of tables

I. Introduction

I.1. Human mesenchymal stem cells (hMSCs)

Human bone marrow-derived mesenchymal stem cells (hMSCs) were first reported by Owen et al. (1988). These cells have the capacity to self-renew and possess multipotentiality, the ability to differentiate into multiple cell types such as adipocytes, osteoblasts, myoblasts, and chondrocytes as shown in Figure 1.1 (Pittenger et al., 1999; Delorme et al., 2006; Uccelli et al., 2008). Due to their multipotency, low immunogenicity and decreased risk of tumorigenesis, hMSCs have become promising candidates for cell therapy in regenerative medicine and tissue engineering (Phinney et al., 2007; Sherman et al., 2011).

Recently, many groups have demonstrated that hMSCs consist of heterogeneous subpopulations defined by their sizes, and each population has different self-renewal and multipotent capacities. As shown in Figure 1.2, three categories of subpopulations, including small rapidly self-renewing (RS) cells (<25 μm), elongated and spindle-shaped (SS) cells (25-40 μm), and slowly replicating, large and flattened (FL) cells (>40 μm), have been defined (Colter et al., 2001; Dominici et al., 2006;

Haasters et al., 2009). Consequently, separation of hMSCs by size has become a very important procedure in stem cell research.

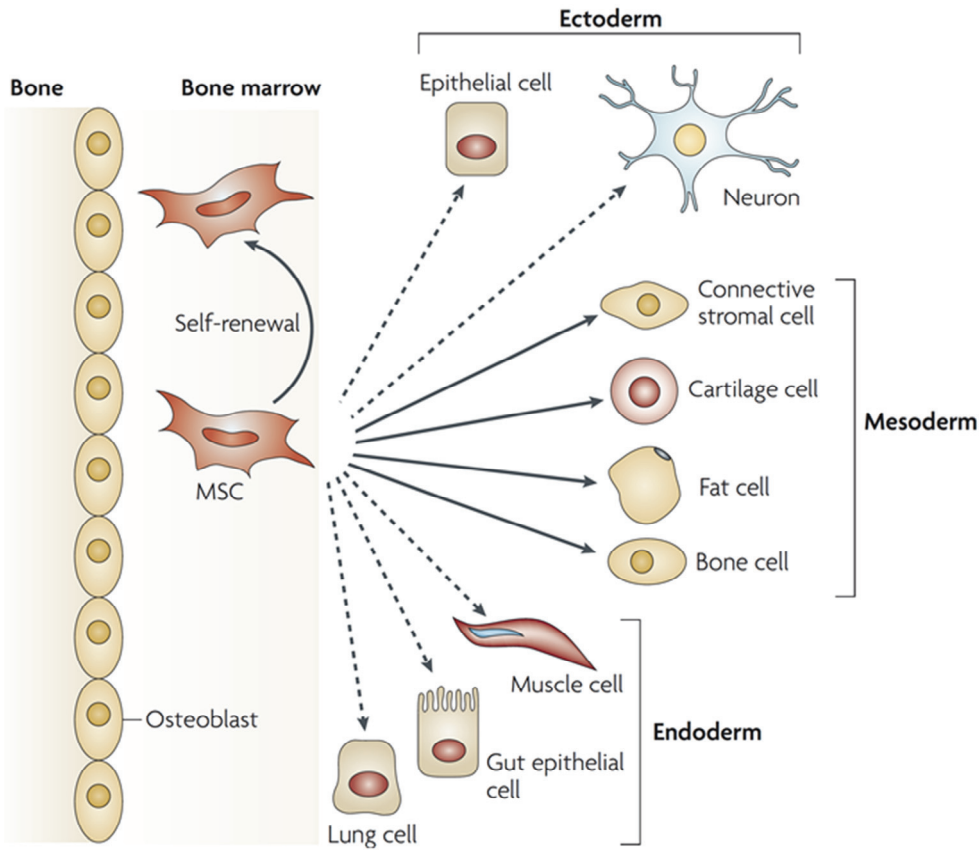

Figure 1.1. The multipotent capacities of MSCs. This figure shows the ability of mesenchymal stem cells (MSCs) in the bone-marrow cavity to self-renew (curved arrow) and to differentiate (straight, solid arrows) towards the mesodermal lineage. The reported ability to transdifferentiate into cells of other lineages (ectoderm and endoderm) is shown by dashed arrows, as transdifferentiation is controversial *in vivo* (Uccelli, et al., 2008).

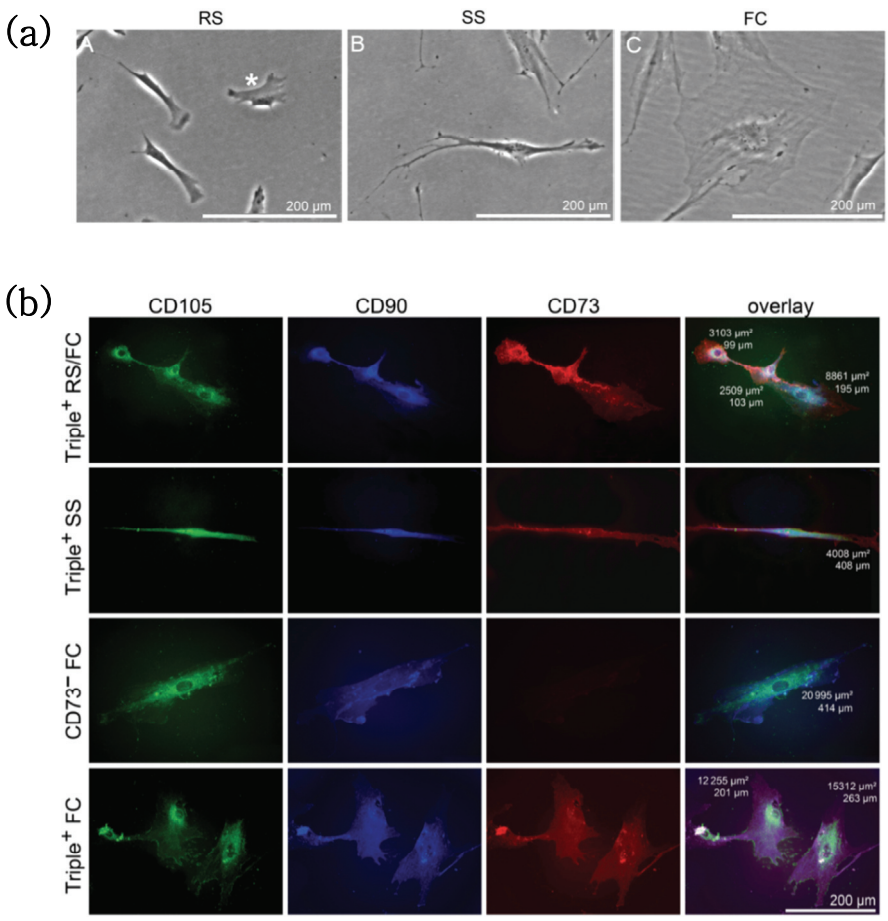

Figure 1.2. Size-dependent characteristics of hMSCs. (a) Phase-contrast images of hMSC culture containing three distinct subpopulations; small rapidly self-renewing (RS) cells, elongated and spindle-shaped (SS) cells, and slowly replicating, large and flattened (FL) cells. (b) Phenotypic characterizations of hMSC subpopulations using multicolor immunofluorescence for surface markers CD105, CD90 and CD73 (Haasters et al., 2009).

I.2. Cell separations in biomedical researches

As a conventional method for separation, fluorescence-activated cell sorting (FACS) has been employed in various studies. Although FACS has shown impressive performance in sorting cells, it is associated with several limitations, including high costs, mechanical complexities, demands for large sample volumes, and the requirement for irreversible fluorescent labeling. Recent advances in microfabrication and microfluidic technologies have complemented the drawbacks of FACS (Whitesides, 2006; West et al., 2008). Based on the mechanism used, microfluidic sorting can be classified as either active or passive separation (Pamme, 2007; Shields et al., 2015). As shown in Figure 1.3, active separation utilizes external forces, such as magnetophoresis, dielectrophoresis, acoustophoresis, and optical methods. Because these methods are known to damage cells, they are not suitable for sorting. On the other hands, passive separation takes advantage of hydrodynamic effects combined with the fluid interaction with the microfluidic channel, and includes inertial force, pinched flow, and hydrodynamic filtration (HDF) (Di Carlo et al., 2007; Kawamata et al., 2008; Yamada et al., 2005).

Among these techniques, HDF is regarded as an efficient sorting method with optimally designed microchannel. Since Seki

and his colleagues first started to study HDF, they have performed separations using a microfluidic device with multi-branched channels for various types of cells including liver cells, white blood cells (WBCs) from red blood cells (RBCs), JM cells (a human T-lymphocyte cell line), and HeLa cells (Yamada et al., 2007). Inertial force-induced separation is also being increasingly used. The Papautsky group designed a simple spiral channel to induce inertial forces, and successfully separated particles and cells by properly bifurcated outlets (Bhagat et al., 2008; Kuntaegowdanahalli et al., 2009). Furthermore, by applying a trapezoidal structure to the spiral channel, Wu et al. (2012) were able to isolate RBCs (<10 μm) from whole blood cells.

Since hMSCs possess different potentials for differentiation according to their size, separation of hMSCs is one of the most important processes in the biomedical research. According to Jung et al. (2015), hMSCs can be sorted into the three subpopulations using a HDF-based microfluidic device. In addition, based on surface marker expression and reverse transcription PCR (RT-PCR) analysis, the RS and SS subpopulations showed higher multipotentiality than did cells in the FL group.

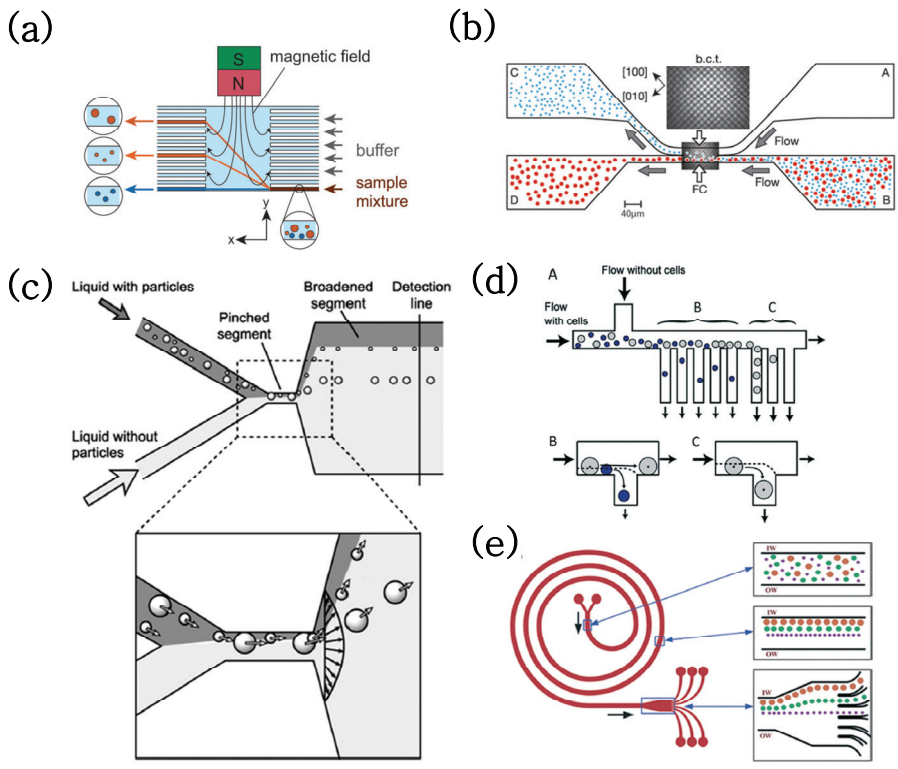

Figure 1.3. Continuous separations in the microfluidic systems. External force is applied in active separation of (a) magnetophoresis and (b) optics (Lenshof et al., 2010). (c–e) Passive separations include pinched flow fractionation (PFF), hydrodynamic filtration (HDF) and inertial focusing.

I.3. Chapter summaries

The purpose of this study is to sort out RS and SS subpopulations of hMSCs from the total hMSC population with high efficiency. Chapter II is dedicated to the design of the microfluidic chip based on the concept of hydrodynamic filtration combined with inertial focusing. By means of microfabrication, the microfluidic chip was made from silicon and glass. With the microchip, microscale experiments were conducted to verify its performances. Experimental methods are described in Chapter III. In Chapter IV, performance of the microfluidic chip was tested. Firstly, fluorescent polystyrene particles were used for the experiment as preliminary tests. Optimal flow conditions for separation were also evaluated using proper sorting systems. Then, hMSCs were pumped into the microfluidic chip to be sorted, and the sorting efficiencies were determined according to the number of hMSCs collected from each outlet.

II. Physical principles of cell / particle separation using the microfluidic chip

To achieve improved sorting efficiency, both hydrodynamic filtration (HDF) and inertial focusing effects in curvilinear microchannel were combined in the microfluidic chip. First, each principle was separately estimated, and then precisely merged into one connected microchannel by considering hydraulic resistances of channel. Here, basic physics of two microfluidic principles behind this technique are demonstrated.

II.1. Hydrodynamic filtration (HDF)

In this study, HDF was applied to the first half of the microfluidic chip for separating heterogeneous hMSCs into subpopulations. The flow-based HDF was accomplished by several capillary branches similar to the mechanism of conventional crossflow filtration. Multi-branches connected to the main channel play a role in removing the fluid gradually introduced from inlets, thereby forcing cells toward the side walls of the main channel, which called focusing (Yamada et al., 2005). The cells are introduced through the main inlet and focused by a side flow injected from a side inlet. Depending on the ratio of the main and side flows, a virtual boundary of the fluid layer between the main

and side flows is formed, which is defined as the cut-off width, W_c. The W_c is a significant term in deciding the standard size of fractionation. Focused cells which have their hydrodynamic center below the W_c will be sloped along the branch channels, whereas larger cells having their hydrodynamic center outside the region are not allowed.

To precisely predict the fractioned boundary width, the flow ratio between each incoming and outgoing stream was derived following consideration of the 3-dimensional flow profile at the rectangular cross-section of the microchannel. For a Newtonian fluid at the steady state laminar flow, the Stokes equation is given as governing equation, $\mu\nabla^2 v = \nabla P$. Then, for a rectangular microchannel with the width W and the height H, the governing equation is substituted for

$$\frac{\partial^2 v_z}{\partial x^2} + \frac{\partial^2 v_z}{\partial y^2} = \frac{1}{\mu}\frac{dP}{dz}. \qquad (1)$$

For a steady state laminar flow, the analytical solution for the velocity profile $v(x,y)$ with a no-slip boundary condition is given as (Yamada et al., 2007)

$$v_z(x,y) = \frac{4H^2}{\pi^3 \mu}\frac{\Delta P}{L}\sum_{n=odd}^{\infty}\frac{1}{n^3}\left[1 - \frac{\cosh(n\pi x / H)}{\cosh(n\pi W / 2H)}\right]\sin(n\pi y / H). \qquad (2)$$

Above, vector v_z is the streamwise axial velocity in the $z-$direction. ΔP is the pressure drop applied along the channel length L and μ stands for the fluid viscosity. As the term n increases over 3, n can be gradually ignored without loss of accuracy.

The volumetric flow rate Q is obtained by integrating Eq.(2) over the width and the height such that (Fuerstman et al., 2007)

$$Q = \frac{WH^3}{12\mu}\frac{\Delta P}{L}\left[1 - \frac{192}{\pi^5}\frac{H}{W}\sum_{n=odd}^{\infty}\frac{1}{n^5}\tanh(n\pi W/2H)\right] = \frac{\Delta p}{R} \qquad (3)$$

where R is the hydraulic resistance.

Moreover, the main channel stream is subdivided and the focused stream of $-X \le x \le 0$ (or $0 \le x \le X$, due to symmetry) with $X = W/2 - W_c$ is set for detailed estimation of flow streams. The fractional flow rate, Q_x, for the focused stream is calculated as

$$\begin{aligned} Q_x &= \int_0^X \int_0^H v_z(x,y)\,dy\,dx \\ &= \frac{WH^3}{24\mu}\frac{\Delta P}{L}\left[\frac{2}{W}X - \frac{192}{\pi^5}\frac{H}{W}\sum_{n=odd}^{\infty}\frac{1}{n^5}\frac{\sinh(n\pi X/H)}{\cosh(n\pi W/2H)}\right]. \end{aligned} \qquad (4)$$

As shown in Figure 2.1, W_c is formed in the front portion of the first branch point where the main and side flows are merged. Since W_c depends on the ratio of the two streams, our previous study confirmed the ratio of flow rates of two stream as the ratio of flow fraction, ξ (Jung et al., 2015). By computing the relationship of

total flow rate and fractional flow rate, $Q_i^m + Q_i^s = Q$ and $Q_i^m + Q_x = Q/2$, ξ can be derived as

$$\xi \equiv Q_i^m / Q_i^s = (Q - 2Q_X)/(Q + 2Q_X). \quad (5)$$

From Eq. (3) with a rapidly converging sum, the flow rate at the main channel between branch point $j-1$ and j can be expressed as

$$Q_{j-1,j}^m \equiv \frac{\Delta P_{j-1,j}^m}{R_{j-1,j}^m} = \frac{WH^3}{12\mu} \frac{\Delta P_{j-1,j}^m}{L_{j-1,j}^m} \left[1 - \frac{192}{\pi^5} \frac{H}{W} \tanh(\pi W / 2H) \right]. \quad (6)$$

The corresponding flow rate $Q_{j-1,j}^m$ is expressed as the output flow at the 1st to $(j-1)$th subtracted from the total input flow Q. Thus, the pressure drop at the interval is estimated as

$$\Delta P_{j-1,j}^m = R_{j-1,j}^m \left(Q - \sum_1^{j-1} Q_j^b \right). \quad (7)$$

Note that the pressure drops between inlet and every outlet point are set to equal on the ground because the main and all branch channels are open to the atmosphere, yielding

$$\Delta P_{i,1} = \cdots = \Delta P_{i,j} = \cdots = \Delta P_{i,O4}. \quad (8)$$

Basically, the pressure drop is the product of the flow rate and hydraulic resistance. With the initial guess of L_1^b, $\Delta P_{i,1}$ is primarily computed, and then for the specific pressure drop value, L_j^b is repeatedly calculated by iteration scheme on the condition of $\Delta P_{i,1} = \Delta P_{i,j}$ in the multi-branches. The minimum tolerance is

established in a nonlinear regression with the least sum of squares method based on generalized reduced gradient scheme.

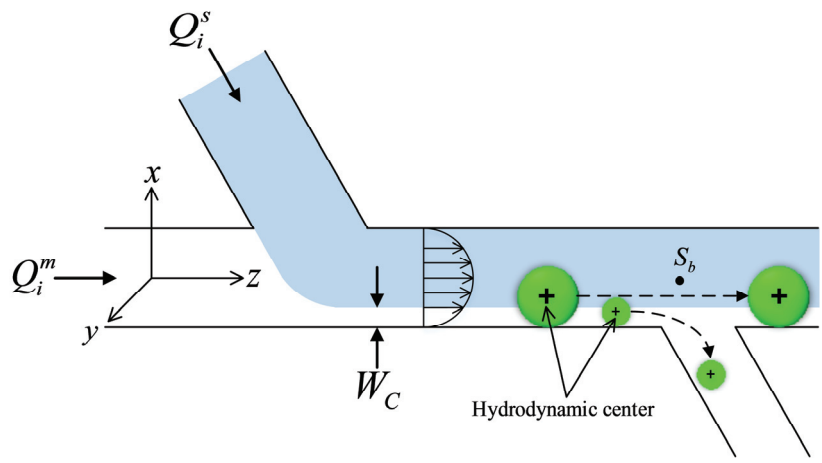

Figure 2.1. Schematic of hydrodynamic filtration (HDF) in a microchannel. In the fully-developed steady state, particles are separated on the basis of the cut-off width (W_C).

II.2. Inertial focusing in the curvilinear channel

In a curvilinear channel, due to the nature of the channel geometry, centrifugal acceleration occurs and causes the formation of two counter rotating vortices on the top and bottom halves of the microchannel cross-section as shown in Figure 2.2. Thus, in a curvilinear channel, fluid flows along the channel forming a helical flow pattern because the fluid basically has a velocity component perpendicular to the normal flow direction. The two counter-rotating vortices are known as Dean vortices. With a dimensionless number, the Dean number (De), the expression of the magnitude of the secondary flows is given by (Dean, 1927)

$$De = \frac{\rho \bar{U} D_h}{\mu} \sqrt{\frac{D_h}{2R_c}} = Re \sqrt{\frac{D_h}{2R_c}} \tag{9}$$

where ρ, $\bar{U}$, μ, and R_c stand for the density of the fluid, average fluid velocity, fluid viscosity and radius of curvature. Re is the flow Reynolds number. For a given Dean number, the average Dean velocity ($\bar{U}_{Dean}$) was calculated as (Ookawara et al., 2006)

$$\bar{U}_{Dean} = 1.8 \times 10^{-4} De^{1.63}. \tag{10}$$

Hence, the Dean drag force (F_D) exerted on the suspended particle by the Dean vortices can be assumed to be (Bhagat et al., 2008)

$$F_D = 3\pi\mu \bar{U}_{Dean} d_p = 5.4 \times 10^{-4} \pi \mu De^{1.63} d_p \tag{11}$$

where d_p is particle diameter. According to the expression above, the magnitude of the Dean drag force is dependent on the size of the particle experiencing the force.

In a plane Poiseuille flow, particles satisfying $d_p / D_h \geq 0.07$ experience a shear gradient induced inertial lift force (F_{SL}) of the parabolic velocity profiles. The F_{SL} forces suspended particle to move towards the channel walls. In addition, the rotational wake around the particles is perturbed because of the presence of the wall. Therefore, particles approaching the wall encounter a wall-induced lift force (F_{WL}) directing them away from the wall. As shown in Figure 2.3, these two oppositely directed lift forces are applied to particles and canceled out, thus equilibrating particles at a distance of $\sim 0.2 D_h$ from the channel wall. Note that particles flowing along the channel are under the continuous influence of the viscous drag force (F_{VD}) parallel to the flow direction (Asmolov, 1999, Di Carlo et al., 2007). The net lift force ($F_L = F_{SL} + F_{WL}$) depends on the position of the particles and can be expressed as (Bhagat et al., 2008)

$$F_L = \rho G^2 C_L d_p^4 \qquad (12)$$

where G is the shear rate of the fluid given by $G = U_{\max} / D_h$, $U_{\max}$ is the maximum fluid velocity and C_L is the lift coefficient. The lift coefficient (C_L) depends on the Reynolds number (Re) and the

position of the particle, not on particle size. That is, all particles regardless of size equilibrate at the same position ($C_L = 0$) for a given *Re*.

Although it is impossible to separate particles based soley on inertial lift force, the additional introduction of a Dean drag force can achieve size-dependent separation in a curvilinear channel. Figure 2.4 shows the positions of particles in a channel cross-section with or without inertial lift force or Dean drag force. At the top and bottom of the microchannel, particles experience a dominant Dean drag force and are entrained in Dean vortices. Near the outer wall, the Dean drag force is supplemented by an inertial lift force, leading the particle to stay entrained in the vortex. At the inner halves of the channel, the Dean drag force and inertial lift force meet in counter directions, and particle equilibrates at the position where the two forces are balanced.

Finally, it must be considered that appropriate ratio of inertial lift force and Dean drag force as (Amini et al., 2014)

$$\frac{F_L}{F_D} \equiv \frac{2d_p^2 R_c}{H^3} > \sim 0.08 . \qquad (13)$$

Particles with a very small F_L/F_D are entrained by one of the Dean vortices because of the dominant Dean drag force, while in the case of F_L/F_D >>20, the inertial lift force is dominant and a

single equilibrium position is not achieved in shorter focusing length. In this study, the above criteria were precisely satisfied to benefit the effects of the Dean flow.

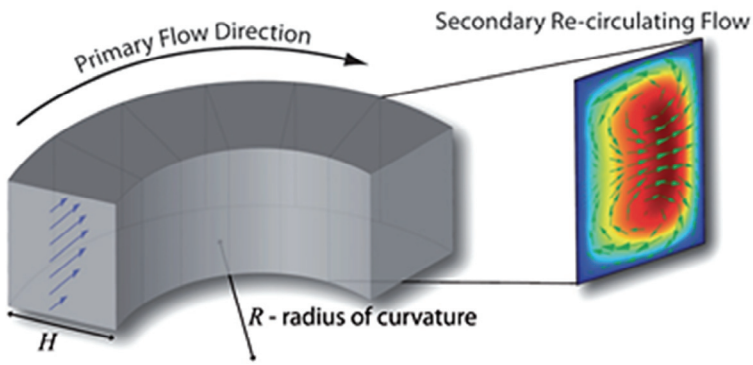

Figure 2.2. Dean vortices in curvilinear channels. In the curvilinear microchannel, faster moving fluid near the channel center tends to continue outward, and to conserve mass, while more stagnant fluid near the walls re-circulates inward. This creates two counter-rotating Dean vortices perpendicular to the primary flow direction (Di Carlo, 2009).

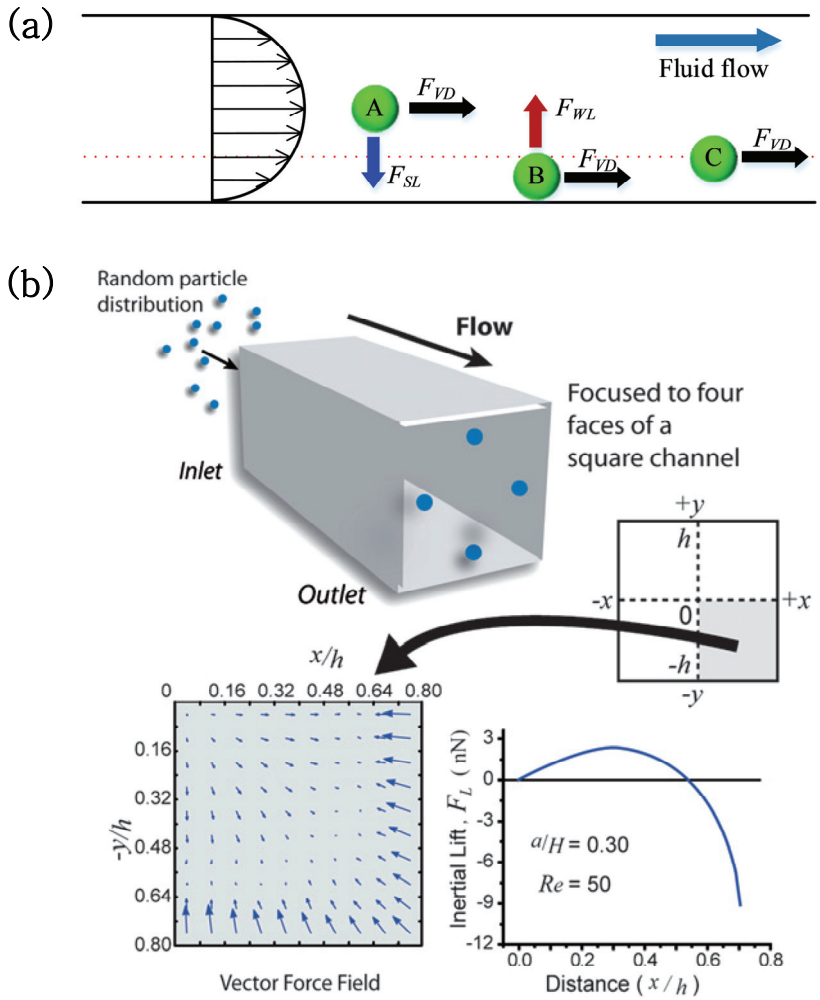

Figure 2.3. Shear gradient (F_{SL}) and wall (F_{WL}) induced lift forces in a rectangular straight channel. (a) Particle at the center of the microchannel **<A>** experiences a dominant F_{SL}. Particle closer to the microchannel wall **<B>** experience a dominant F_{WL}. These oppositely directed forces cancel out and thus the particles equilibrate at a distance of ~$0.2D_h$ from the channel wall indicated by the red dotted line. (Bhagat, 2008; Di Carlo, 2009).

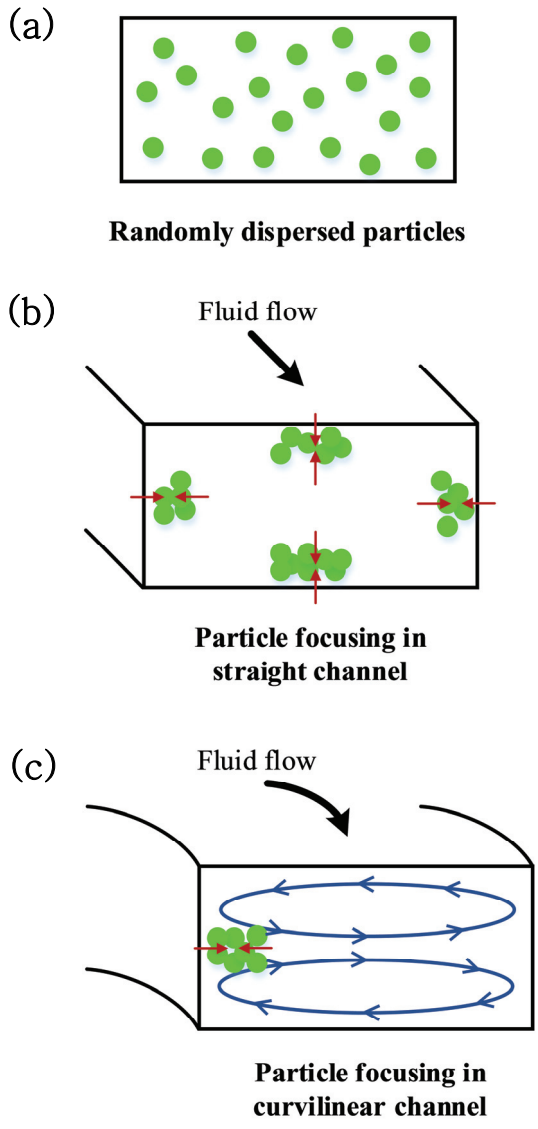

Figure 2.4. Effects of inertial lift (F_L) and Dean drag (F_D) forces on the particles. (a–b) In the rectangular straight channel, randomly dispersed particles are focused near the channel wall by F_L (red arrow), and (c) further focused near the inner center wall when additional F_D (blue circulating arrow) is applied in the curvilinear channel.

III. Hybrid microfluidic chip combined with inertial focusing and hydrodynamic filtration (HDF)

To sort the RS and SS subpopulation from the total hMSCs population, the microfluidic chip used in this study was designed precisely based on channel networks for HDF and inertial focusing. In this chapter, the configuration of the microfluidic chip, fabrication, and sorting operation methods are described.

III.1. Microchannel design

The microfluidic chip was designed based on the principles of hydrodynamic filtration and inertial focusing. The microfluidic chip contained 25 multi-branches and 2 spiral channels of rectangular cross-section (Figure 3.1). The multi-branched channels (50 μm wide and 90 μm high) for HDF are located in the early microchannel part, resulting in preliminarily filtering of small hMSCs (RS and SS subpopulations) among the total population of hMSCs. Once hMSCs are separated in multi-branched channels, the cells are secondarily purified by inertial focusing in spiral channels with properly adjusted flow resistances located at the end of the multi-branched channels (500 μm wide and 90 μm high) and main channel (200 μm wide and 90 μm high). Detailed parameters and values for the microchannel are summarized in Table 1.

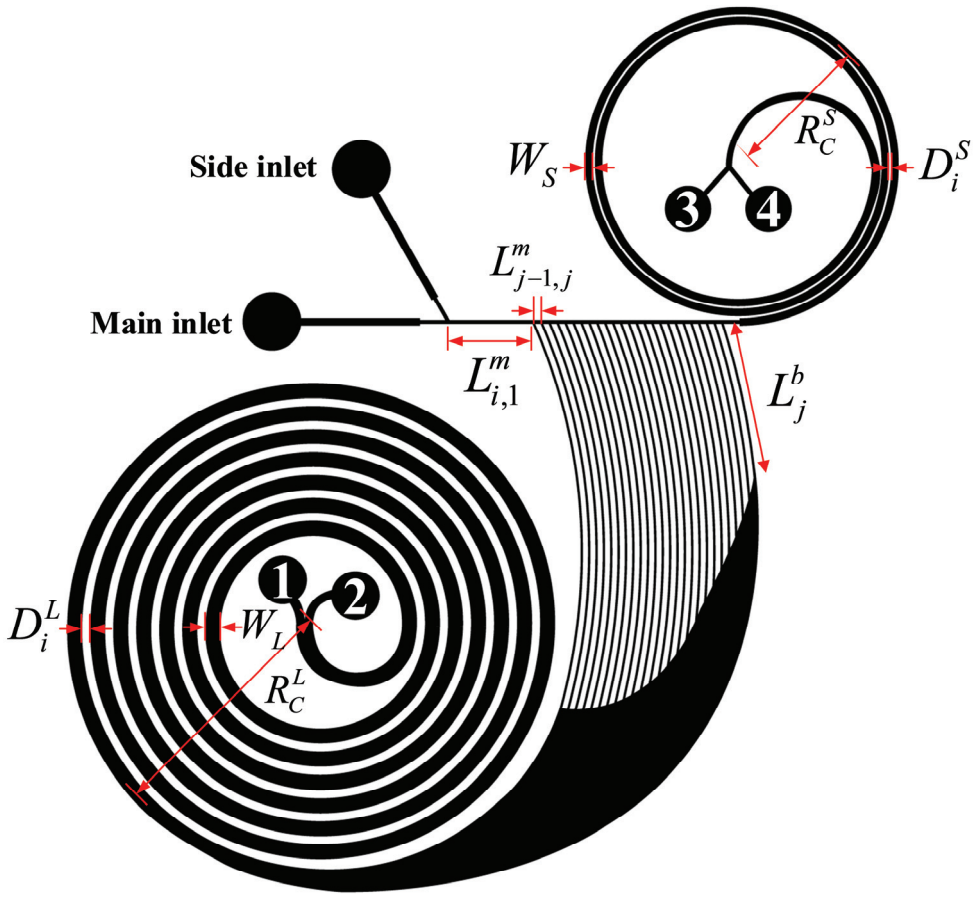

Figure 3.1. Schematic of the microchannel used for sorting hMSCs.

Table 1. Design parameters and values of the microfluidic chip

Channel	Dimension	Notation	Values(μm)
Main	Height	H	90
	Width	W	100
	Length	$L_{i,1}^{m}$	2000
		$L_{j-1,j}^{m}$ $(j = 1\text{-}25)$	187.6
	Cut-off	W_C	20
Branch	Height	H	90
	Width	W_j^b	50
	Length	L_j^b $(j = 1\text{-}25)$	to be computed
Large spiral	Height	H	90
	Width	W_L	500
	Length	L_L	244000
	Radius of curvature	R_C^L	7500
	Inter-channel distance	D_i^L	250
	Turn	T_L	7
	Bifurcated width	W_{O1}, W_{O2}	300, 200
Small spiral	Height	H	90
	Width	W_S	200
	Length	L_S	74455.8
	Radius of curvature	R_C^S	5000
	Inter-channel distance	D_i^S	100
	Turn	T_S	2.5
	Bifurcated width	W_{O3}, W_{O4}	100

The chip consists of two inlets, one for injecting prepared sample suspensions parallel to the direction of the main flow, and the other for injecting cell-free medium needed to focus samples toward the opposite wall. In the steady state, the parabolic velocity profile with a fully-developed flow is observed at the distance of approximately $Re(0.1r_h)$ from the node of the main and side channels, where r_h is the equivalent hydraulic radius, and Re means Reynolds number. Small cells whose hydrodynamic centers are located in the W_c are diverted into the following branch channels at an angle of 60° , while large cells pass the branch channel and migrate along the main channel. In the microfluidic chip, W_c is considered to be 20 μm to exclude the FL (> 40 μm) subpopulation of hMSCs (Figure 3.2).

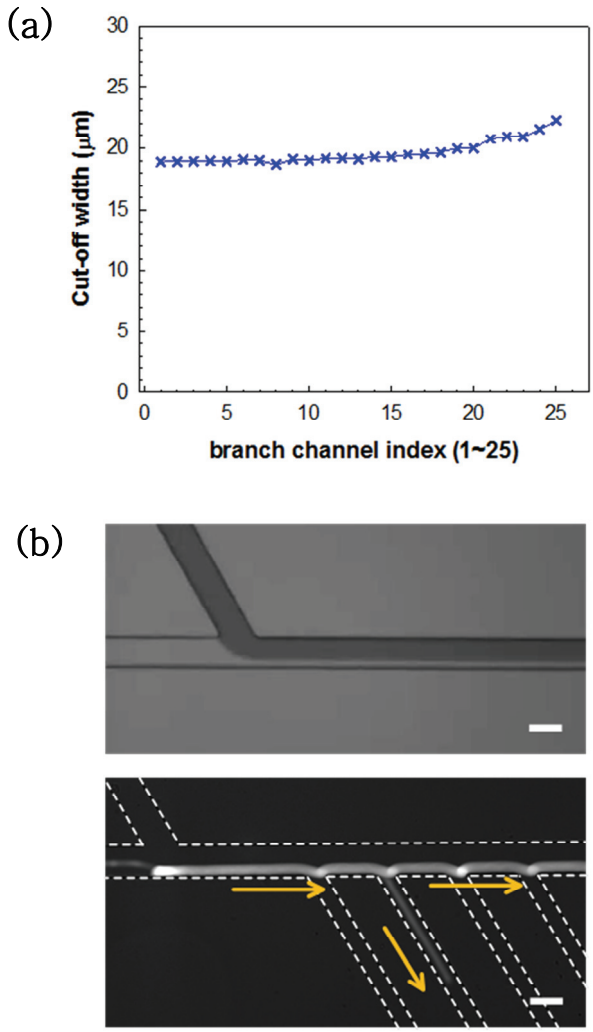

Figure 3.2. Visualization of the virtual boundary of the fluid flow (W_C). (a) Based on HDF principles, W_C was calculated as an average 19.9 μm. (b) The stream line of W_C was visualized by flowing trypan blue dye. The fluorescent particle streak shows successful separation of HDF. (Scale bar: 100 μm).

III.2. Microfluidic chip fabrication

To make the microfluidic chip, a master mold for a polydimethylsiloxane (PDMS; Sylgard 184, Dow Corning, MI) replica was fabricated by means of the standard soft lithography of the MEMS process as shown in Figure 3.3 and Table 2. The layouts of the channels were drawn with AutoCAD (Autodesk Inc.), and were reverse-printed on the plastic photomask film (Figure 3.4a).

The Si wafer (boron doped, p-100) was cleaned by the plasma asher (Microwave Plasma Asher, Germany), and spin-coated with SU8-2050 (Microchem, MA), a negative photoresist (PR). Microchannel patterning on the PR coated wafer was performed by photolithography. Then, the unexposed PR was removed by SU8-developer (Microchem, MA). The manufactured master mold was inspected by Alpha step (ASIQ, KLA-TENCOR, CA), and the results are presented in Figure 3.4b. To make a PDMS replica with the designed patterns, a silicon elastomer prepolymer base and curing reagent mixture at a volume ratio of 10:1 was poured on the master mold, and then the air bubbles were sufficiently degassed in a vacuum chamber. The PDMS replica was cured at 80℃ for at least 1 hr. The peeled PDMS replica was punched to generate holes for inlets and outlets. The

patterned side of the PDMS replica and one side of the cleaned slide glass were treated with air plasma at 80W for 40 sec using an O_2 plasma generator (CUTE-1MP, FemtoScience, Korea), and immediately bonded following the post-baking for 1 hr.

Table 2. Conditions for procedure of master mold fabrication

No.	Step	Process	Condition
1	Substrate pretreatment	plasma asher	150 W, 1 min
2	Photoresist	speed 1	500 rpm, 10s
		speed 2	1750 rpm, 30s
		speed 3	500 rpm, 10s
3	Soft bake	Temp. 1	65℃, 5 min
		Temp. 2	95℃, 15 min
		Temp. 3	65℃, 2 min
4	Exposure	MA6II ($15\ mW/cm^2$)	14.7 s ($220\ mJ/cm^2$)
5	Post exposure bake (PEB)	Temp. 1	65℃, 5 min
		Temp. 2	95℃, 10 min
6	Development	SU8-Developer	7 min
7	Rinse & Dry	IPA, DI water	Briefly

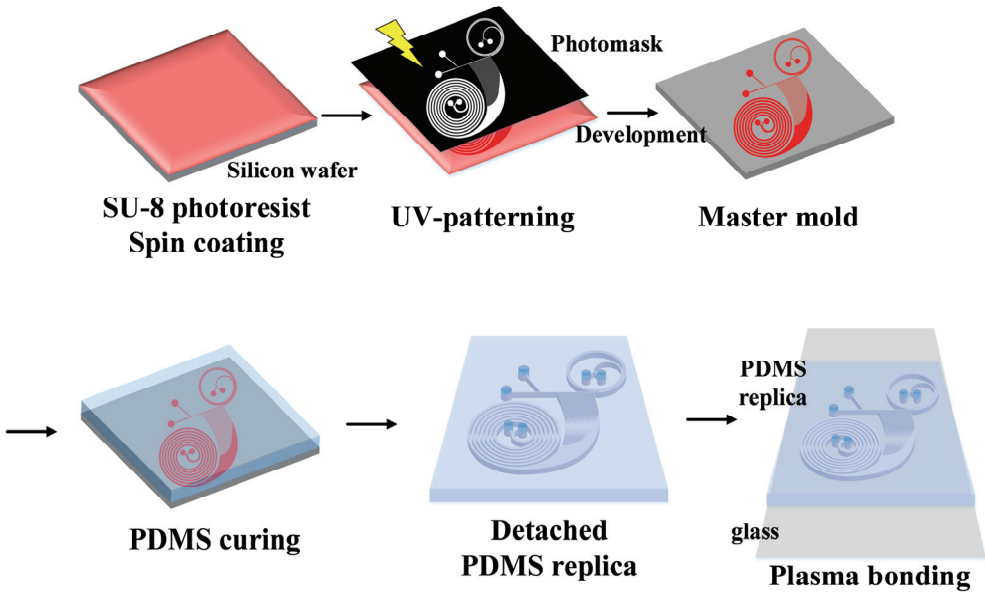

Figure 3.3. Schematic illustrating the fabrication procedures for the master mold and PDMS-glass chip.

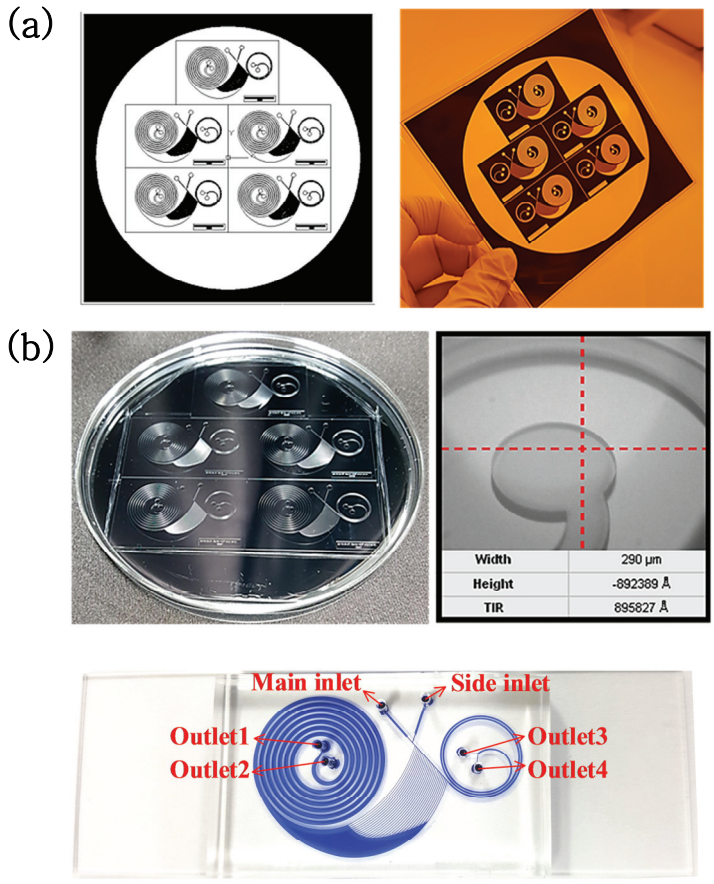

Figure 3.4. AutoCAD drawing for the film mask and fabricated master mold. Inspection of the master mold was achieved using alpha step and up-light microscope. The completely fabricated PDMS-glass chip is shown at the bottom.

III.3. hMSC preparations

Adult bone marrow-derived hMSCs were purchased (Cambrex, MD), and cultured at 37℃ with 5% CO_2 at a density of 4.0×10^4 cells/100mm dish (Corning Inc., NY). To culture hMSCs, Dulbecco's modified Eagle's medium (DMEM)-low glucose (WelGENE, Korea) supplemented with 10% fetal bovine serum (FBS; Gibco, CA) and 1% penicillin/streptomycin (Gibco, CA) was used. Prior to separation, the areas and equivalent diameters for the size-distribution of heterogeneous hMSCs were analyzed in the suspended states (Figure 3.5). The equivalent diameter d ($=\sqrt{L_l L_s}$) is reasonably calculated by 2-dimensional ellipsoidal particle with a major axis L_l (the longest length) and minor axis L_s (the shortest length).

III.4. Sorting operation for the microfluidic chip

Before sorting experiments were carried out, the microfluidic chip was washed with the cell- or particle-free filtered suspensions through 0.2-μm syringe filters (Sartorius, Japan) at 30 μL/min for 30 min and filled with the solutions to maintain a hydrophilic environment.

The prepared sample suspensions were then continuously introduced into the microchannel through the main inlet using the main syringe pump (Pump11 Elite Single Syringe, Harvard Apparatus, MA), while the cell- or particle-free solutions were injected as sheath flows through a side inlet using another syringe pump (KDS-200, KD Scientific, MA), as shown in Figure 3.6. The total flow rate (Q_t) was 500 μL/min and the ratio of the side flow rate (Q_s) to main flow rate (Q_m) was fixed at 6.

In the sorting system, an inverted microscope (Eclipse TE2000-U, Nikon, Japan) was positioned to monitor and capture images of microfluidic chip separation. Images and particle streak images were taken by digital 5M pixel sCMOS camera (Zyla, ANDOR, UK). Especially, particle streak images were captured at an exposure time of 80 ms with NIS-elements software, and at least 10 images were superimposed by ImageJ (NIH, MD). All shown data were obtained from at least 3 replicates of the experiments and were analyzed by ImageJ.

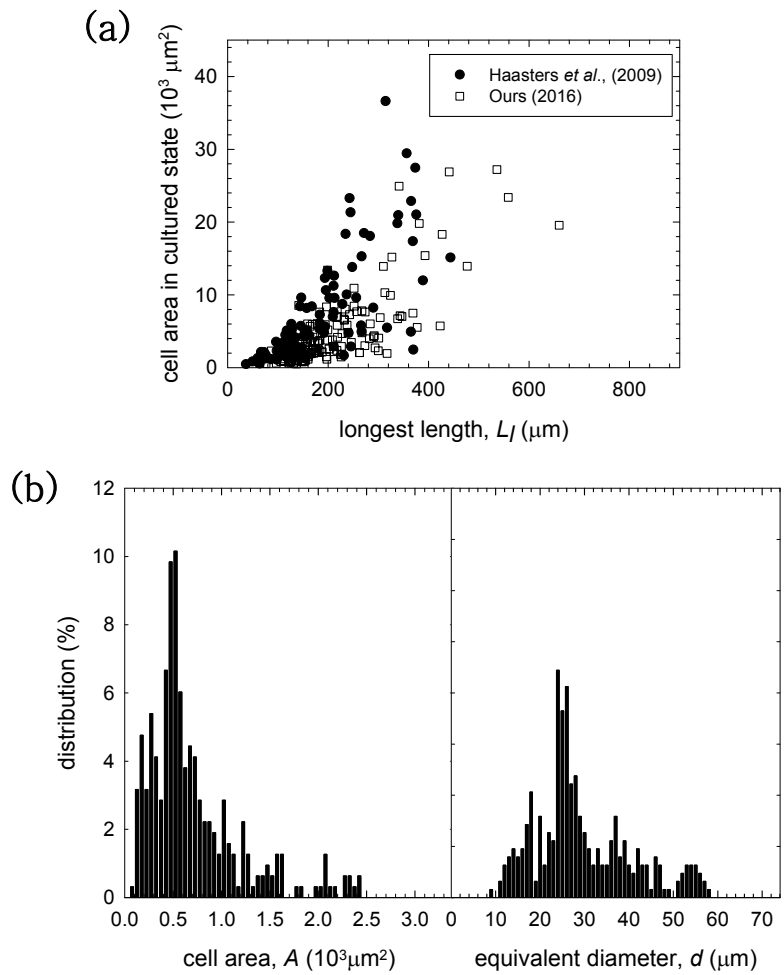

Figure 3.5. Size-distribution of the hMSCs. (a) Relationship between major axis and 2-D area of hMSCs in cultured state compared with previously published data (Haasters et al., 2009), (b) distribution of suspended hMSCs based on their 2-dimensional area and its equivalent diameter.

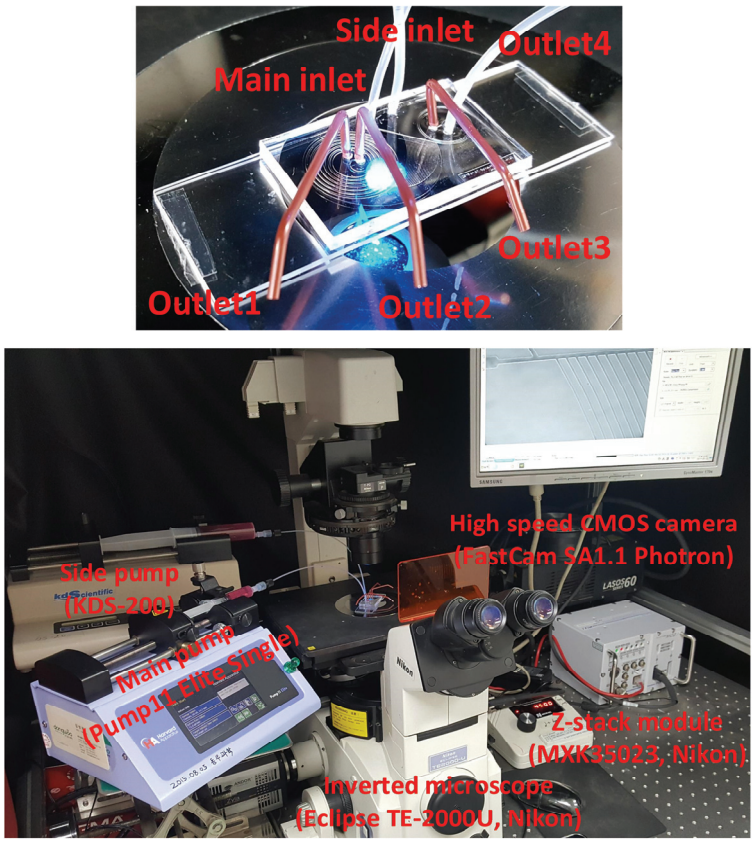

Figure 3.6. Sorting systems with the microfluidic chip connected to pumps via tubing under microscope.

IV. Size-dependent separation of hMSCs by applying microfluidic chip

IV.1. Fluorescent polystyrene particle separation

Prior to the size dependent separation of hMSCs, we performed preliminary tests to examine the device performance using the fluorescent polystyrene particle suspensions of 15 and 39 μm (36-4 and 35-7, Thermo Fisher Scientific Inc., US) dispersed in pre-filtered 0.2% TritonX-100 aqueous solution (50 ppm). Bidispersed particle suspensions were gently mixed using a magnetic stirrer for 30 min followed by sonication for 30 sec to prevent the aggregation of particles. The mixed particle suspensions were evaluated under a microscope before injection into the microfluidic chip.

To confirm the particle focusing in the spiral channel, the trajectories of particles were observed. Figure 4.1 shows the composite images created by superimposing photographs taken at each channel loop and outlet section. The 15-μm particles (red) migrated into the outer half of the channel, while the 39-μm particles (green) equilibrated near the inner wall. The images of sorted particles in each outlet are shown in Figure 4.2. As

mentioned in the data, most large 39−μm particles were collected from outlet 4, and the 15−μm small particles were found predominantly in outlets 1 and 3.

To evaluate the separation efficiency, the obtained images were analyzed by ImageJ and the results were plotted as recovery and purity (Figure 4.3). The purity in each outlet demonstrates the ratio of the number of cells to the total number of cells in each outlet. Recovery represents the ratio of the number of desired cells that accumulated in each outlet to the total number of target cells in all outlets. As shown in Figure 4.3a, a recovery of ca. 99% in separating 39−μm particles was observed, and the purity of 15−μm particles from outlets 1 and 3 was determined to be 99%.

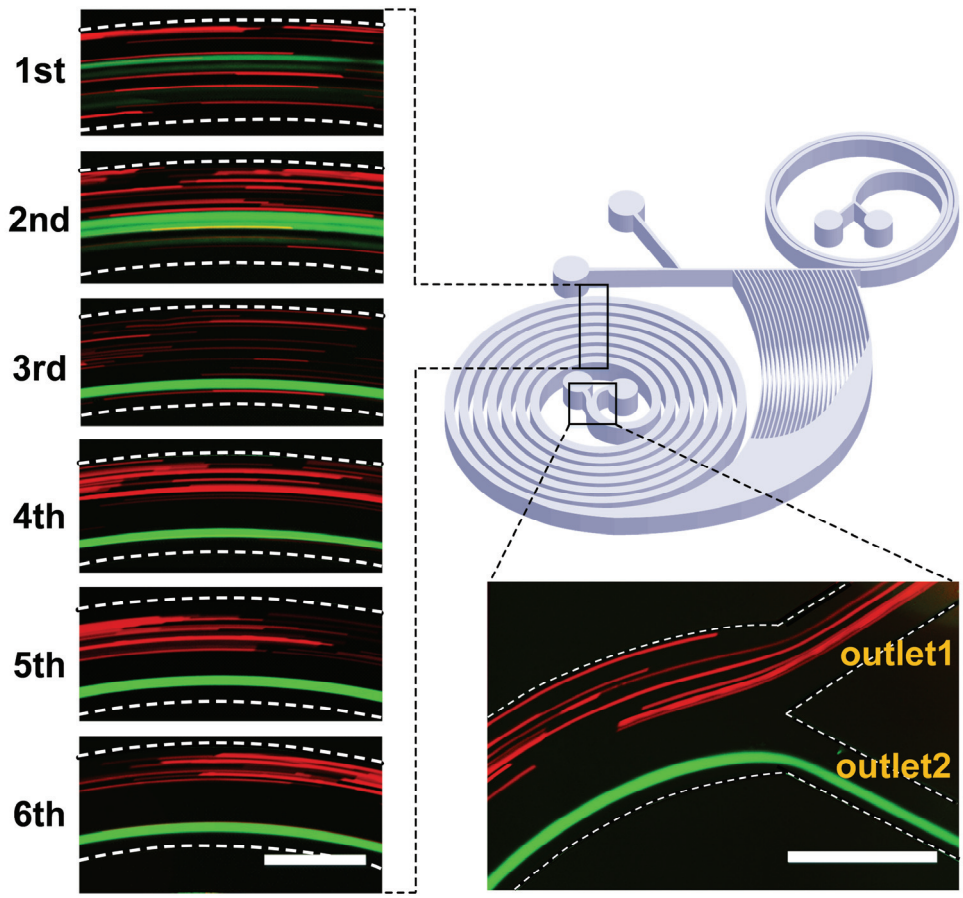

Figure 4.1. Superimposed fluorescent particle trajectories. The panels represent the 500 μm wide spiral channels along the loops and bifurcated outlets. (Scale bar: 500 μm).

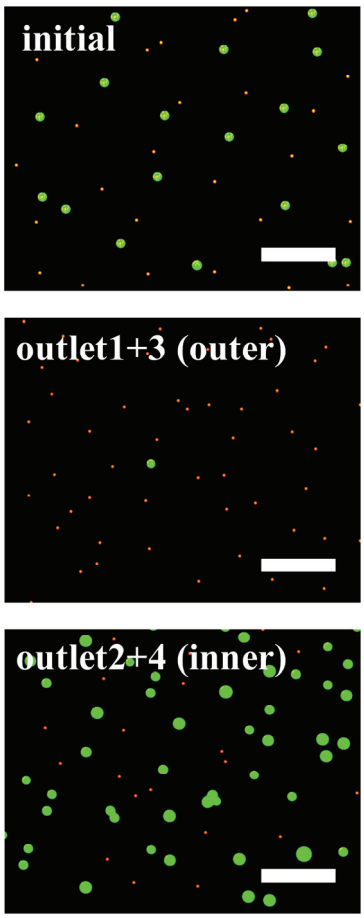

Figure 4.2. Fluorescent images of particles collected from the outlets. The 30 ppm bidispersed particle suspension in 0.2% (w/v) TritonX-100 was separated by using the microfluidic chip; 15- and 39-μm particles are represented by red and green fluorescence, respectively. (Scale bar: 200 μm).

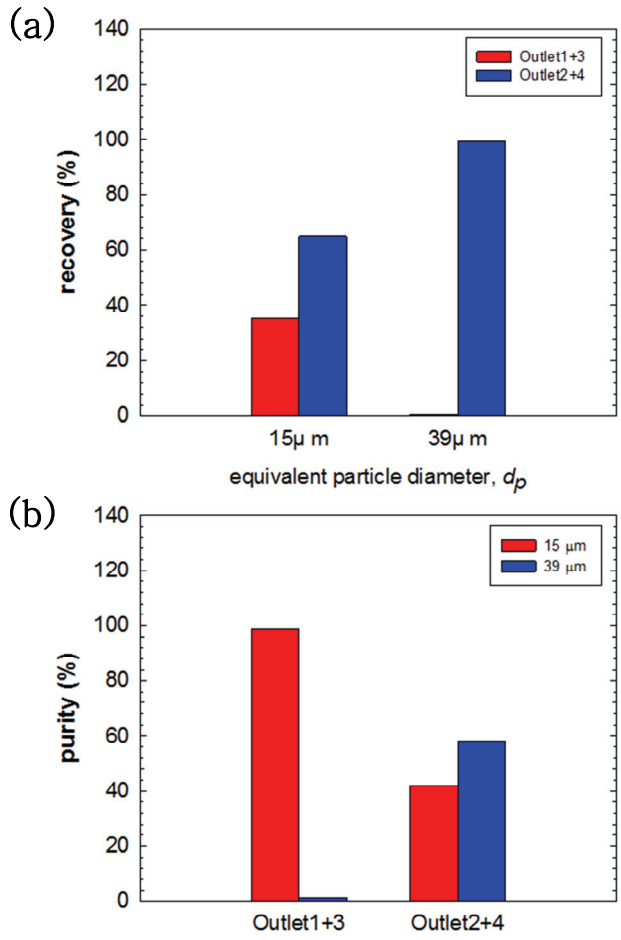

Figure 4.3. Sorting results of the model particles using the microfluidic chip. (a) Most of the large (39−μm) particles were collected from outlets 2 and 4. (b) In outlets 1 and 3, small (15−μm) particles with a purity of up to 99% were observed.

IV.2. Separation of hMSCs

To sort hMSCs using the microfluidic chip, flow stabilization was conducted before the administration of cells into the microchannel to avoid air bubble trapping. A filtered cell-free medium was introduced to the main and side inlets for 15-30 min at 30 μL/min. After stabilization, the medium was allowed to remain in the microchannel to maintain an environment in the channel similar to the culture environment.

The hMSCs were suspended at a density of 10^5 cells/mL in DMEM. To accurately evaluate the sorting efficiency, cell separation was not examined before the flow profile was stable. If air bubbles became trapped in the channel during the experiment, the syringe pump used for main flow injecting cells was stopped, and the air bubbles were removed by introducing high flows from the side input.

With consistent flow inputs of 71.4 μL/min for the main flow and 428.6 μL/min for the side flow, hMSC separation was continuously performed. Sorted hMSCs from each outlet were collected and captured for analysis using ImageJ. Figure 4.4 shows the hMSCs after collection from the outlets. Average sizes of cells presented in the histogram of the size distribution were 23.2 μm and 43.6 μm from outlets 1+3 and 2+4, respectively (Figure 4.5).

Based on the cell sizes corresponding to their equivalent diameters, the sorted hMSCs were analyzed for separation efficiency, represented as recovery and purity. As shown in Figure 4.6, recoveries of ca. 83% and 98% were observed, and the purity of each outlet was determined to be 99% and 76%, respectively. These data prove that the microfluidic chip can separate large cells belong to the FL subpopulation from heterogeneous hMSCs.

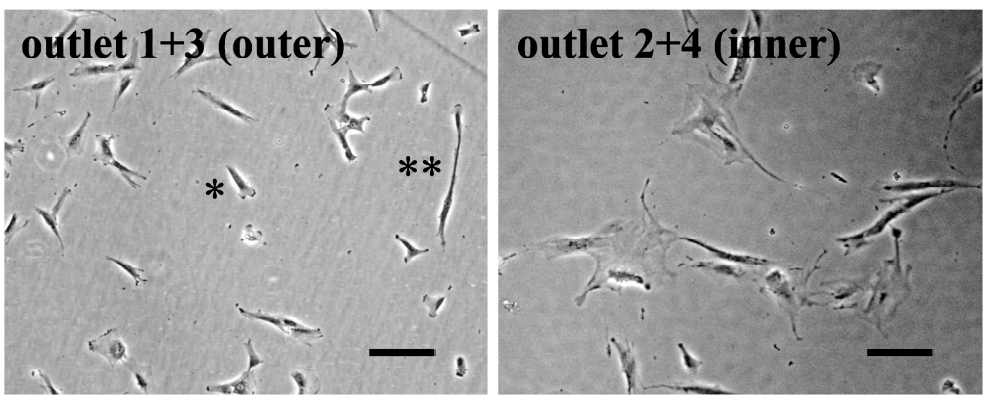

Figure 4.4. Images of hMSCs collected from the outlets. Appearances of the hMSC in culture are distinguishable according to the size-dependent subpopulations. From outlets 1 and 3, RS and SS cells are observed and marked as * and **, respectively. FL cells dominantly occupy outlets 2 and 4. (Scale bar: 100 μm).

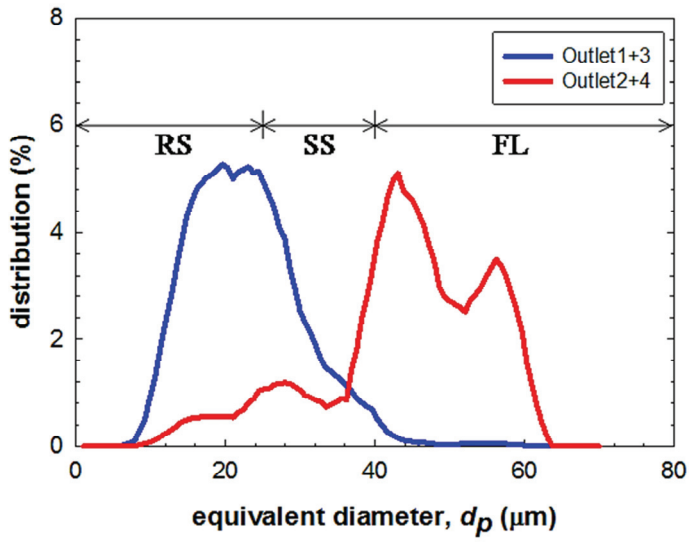

Figure 4.5. Size distribution of hMSCs after sorting. The RS, SS, and FL subpopulations are defined as suspended sizes of <25 μm, 25−40 μm, and >40 μm, respectively. hMSCs collected from outlets 1 and 3 belong to RS and SS subpopulations while hMSCs from outlets 2 and 4 are classified as belonging to the FL subpopulation.

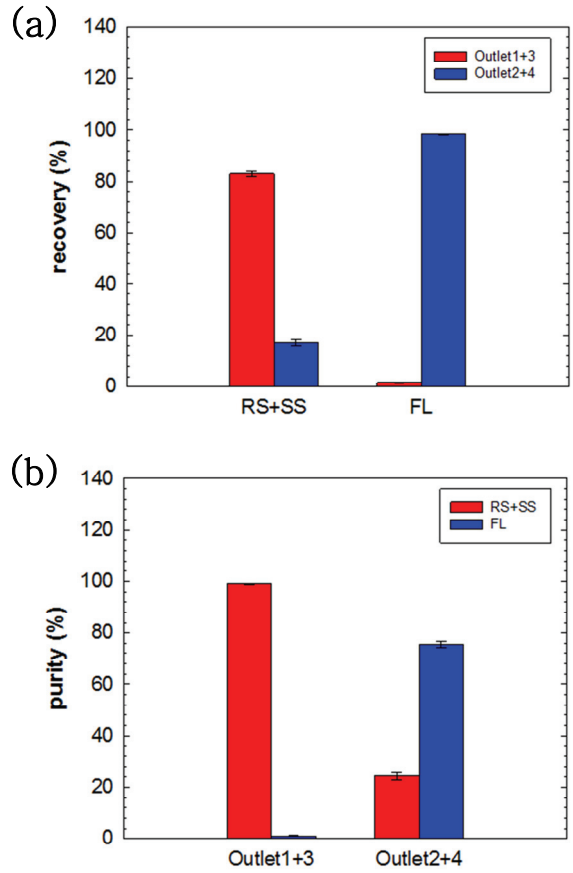

Figure 4.6. Sorting efficiencies of hMSCs using the microfluidic chip. The performance of the microfluidic chip is assumed by (a) recovery and (b) purity according to the outlets.

IV.3. Viability and growth rate of subpopulations

Due to the velocity gradients in the flow fields, shear stress, which is highly related to the mortality of cells, is applied to cells in the microchannel proportional to the flow rate (Q). Thus, to confirm cell viability, the sorted populations from each outlet were assessed via the trypan blue (15250-061, Gibco, CA) exclusion test before and after the separations. Cell viability is the ratio of viable cells to the total number of cells on the grids on the hemocytometer. In addition, the growth rates of different subpopulations were investigated for 7 days to verify the self-renewal of hMSCs. 150 cells from each population were seeded on a 96-well culture plate, and the cell numbers were counted with trypan blue staining solution on once every second day. Doubling time (T_D) can be assumed as

$$T_D = t\left[\ln 2 / \ln(N_F / N_B)\right], \tag{14}$$

where t is incubation time, N_B and N_F are the cell number at the beginning and end of the incubation time, respectively.

As demonstrated in Figure 4.7, the viabilities of the sorted hMSCs were 89.9% and 90.5% corresponding to small and large subpopulations, respectively. Compared to unsorted hMSCs, there was no significant difference in the viabilities of these subpopulations. The viabilities in our study were slightly lower

than in the previous study (Jung et al., 2015), but the sorting process did not cause any critical cell damage. Furthermore, the doubling times of small cells and large cells were 7.4 and 12.2 days, respectively. The growth rate of the small cells was faster than that of the large cells, as shown in Figure 4.7b.

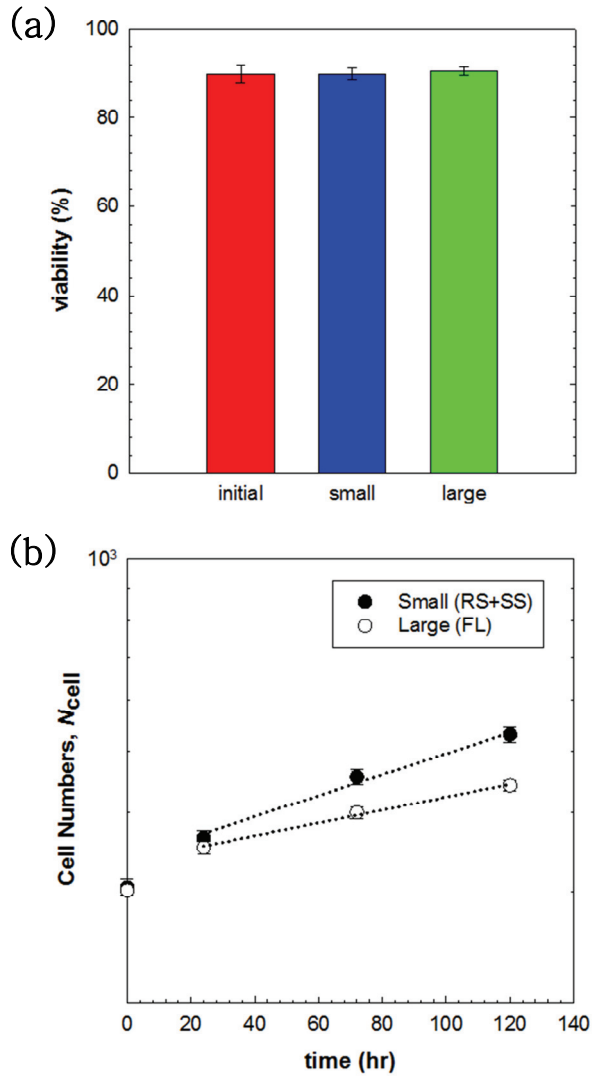

Figure 4.7. Viability and growth rate of separated hMSCs. (a) Viability of sorted cells, and (b) growth rate of accumulated sorted cells for the small and large subpopulations.

Ⅴ. Conclusions

Stem cells are defined as undifferentiated cells possessing self-renewal and capacity to differentiate into specialized cell types. In the fields of regenerative medicine, stem cell therapy have become promising treatments for intractable diseases including nerve injuries, severe tissue damages, defects in immune systems, etc (Uccelli et al., 2008). Especially, hMSCs are considered to be splendid cell source due to many advantages mentioned above. However, utilization of hMSCs in cell therapy is ambiguous because of their size-dependent heterogeneous characteristics. Therefore, separation and isolation of target cells with high potential from the total population is very important.

In order to separate hMSCs, we designed the microfluidic chip based on hydrodynamic filtration and inertial focusing principles. By introducing polystyrene particles, we observed the trajectories of particle streaks in each channel to test whether it works. Particles that are primarily filtered by HDF were focused in equilibrium positions as migrating along the spiral loops. The 15-μm diameter particles experienced a dominant Dean drag force, and entrained in one of the two Dean vortices. The 39-μm diameter particles experienced a dominant inertial lift force and thus equilibrated at the inner microchannel wall. With properly

bifurcated outlets, isolation of 39-μm particles was achieved completely as shown in figure 4.3. According to Di Carlo (2009), channel length required for focusing to equilibrium positions is reversely proportional to square of particle diameter. Thus, by adjusting channel length and appropriately bifurcated outlets, the microfluidic chip can separate smaller particles with improved resolution.

Sorting of hMSCs was also accomplished efficiently with high relative viabilities (>90%). Most of cells belong to the FL group were filtered by multi-branches, and traveled along the main channel to the small spiral channel for further separation. The FL group is isolated up to 100% from outlets 2 and 4. After sorting, the small cells were observed in outlets 1 and 3, while the large cells occupied outlets 2 and 4. Due to the small cells were entrained to one of the Dean vortices, some of the RS and SS subpopulations exited through outlets 2 and 4 as well as outlets 1 and 3. However, this purity can be improved by serial sorting, modulation of detailed flow condition and channel length.

In conclusion, we acquired target subpopulations enriched from the total hMSCs using the microfluidic chip with hydrodynamic filtration combined with inertial focusing, which is promising technique for various stem cell research fields.

References

Amini H, Lee W, Di Carlo D (2014). "Inertial microfluidic physics." Lab Chip 14: 2739-2761.

Asmolov ES (1999). "The inertial lift on a spherical particle in a plane Poiseuille flow at large channel Reynolds number." J Fluid Mech 381: 63-87.

Bhagat AA, Kuntaegowdanahalli SS, Papautsky I (2008). "Continuous particle separation in spiral microchannels using dean flows and differential migration." Lab Chip 8: 1906-1914.

Colter DC, Sekiya I, Prockop DJ (2001). "Identification of a subpopulation of rapidly self-renewing and multipotential adult stem cells in colonies of human marrow stromal cells." Proc Natl Acad Sci U S A 98(14): 7841-7845.

Dean WR, Hurst JM (1927). "Note on the motion of fluid in a curved pipe." Phil Mag Ser 4: 208-223.

Di Carlo D, Irimia D, Tompkins RG, Toner M (2007). "Continuous inertial focusing, ordering, and separation of particles in microchannels." Proc Natl Acad Sci U S A 104:18892-18897.

Di Carlo D (2009). "Inertial microfluidics." Lab Chip 9: 3038-3046.

Delorme BS, Chateauvieux, et al. (2006). "The concept of mesenchymal stem cells." Regen Med 1(4): 497-509.

Dominici M, Blanc KL, Mueller I, Slaper-Cortenbach I, Marini FC, Krause DS, Deans RJ, Keating A, Prockop DJ, Horwitz EM (2006). "Minimal criteria for defining multipotent mesenchymal stromal cells. The

International Society for Cellular Therapy position statement." Cytotherapy 8: 315-317.

Fuerstman MJ, Lai A, Thurlow ME, Shevkoplyas SS, Stone HA, Whitesides GM (2007). "The pressure drop along rectangular microchannels containing bubbles." Lab Chip 7: 1479-1489.

Haasters F, Prall WC, Anz D, Bourquin C, Pautke C, Endres S, Mutchler W, Docheva D, Schieker M (2009). "Morphological and immunocytochemical characteristics indicate the yield of early progenitors and represent a quality control for human mesenchymal stem cell culturing." J Anat 214(5): 759-767.

Jung H, Chun M-S, Chang M-S (2015). "Sorting of human mesenchymal stem cells by applying optimally designed microfluidic chip filtration." Analyst 140: 1265-1274.

Kawamata T, Yamada M, Yasuda M, Seki M (2008). "Continuous and precise particle separation by electroosmotic flow control in microfluidic devices." Electrophoresis 29: 1423-1430.

Kuntaegowdanahalli SS, Bhagat AA, Kumar G, Papautsky I (2009). "Inertial microfluidics for continuous particle separation in spiral microchannels." Lab Chip 9: 2973-2980.

Lenshof A, Laurell T (2010). "Continuous separation of cells and particles in microfluidic systems." Chem Soc Rev 39: 1203-1217.

Ookawara S, Street D, Ogawa K (2006). "Numerical study on development of particle concentration profiles in a curved microchannel." Chem Eng Sci 61: 3714-3724.

Owen M, Friedenstein AJ (1988). "Stromal stem cells: marrow-derived osteogenic precursors." Ciba Found Symp 136: 42-60.

Pamme N (2007). "Continuous flow separations in microfluidic devices." Lab Chip 7: 1644-1659.

Phinney DG, Prockop DJ (2007). "Concise Review: Mesenchymal Stem/Multipotent Stromal Cells: The State of Transdifferentiation and Modes of Tissue Repair-Current Views." Stem Cell 25: 2896-2902.

Pittenger MF, Mackay AM, Beck SC, Jaiswal RK, Douglas R, Mosca JD, Moorman MA, Simonetti DW, Craig S, Marshak DR (1999). "Multilineage Potential of Adult Human Mesenchymal Stem Cells." Science 284(5411): 143-147.

Sherman LS, Munoz J, Patel SA, Dave MA, Paige I, Rameshwar P (2011). "Moving from the Laboratory Bench to Patients' Bedside: Considerations for Effective Therapy with Stem Cells." Clin Transl Sci 4: 380-386.

Shields W, Reyes CD, López P (2015). "Microfluidic cell sorting: a review of the advances in the separation of cells from debulking to rare cell isolation." Lab Chip 15: 1230-1249.

Uccelli A, Moretta L, Pistoia V (2008). "Mesenchymal stem cells in health and disease." Nat Rev Immonol 8: 726-736.

Wang X, Chen S, Kong M, Wang Z, Costa KD, Li RA (2011). "Enhanced cell sorting and manipulation with combined optical tweezer and microfluidic chip technologies." Lab Chip 11: 3656-3662.

West J, Becker M, Tombrink S, Manz A (2008). "Micro Total Analysis Systems: Latest Achievements." Anal Chem 80: 4403-4419.

Whitesides GM (2006). "The origins and the future of microfluidics." Nature 442:368-373.

Wu L, Guan G, Hou HW, Bhagat AA, Han J (2012). "Separation of Leukocytes from Blood Using Spiral Channel with Trapezoid Cross-Section." Anal Chem 84: 9324-9331.

Yamada M, Seki M (2005). "Hydrodynamic filtration for on-chip particle concentration and classification utilizing microfluidics." Lab Chip 5: 1233-1239

Yamada M, Kano K, Tsuda Y, Kobayashi J, Yamato M, Seki M, Okano T (2007). "Microfluidic devices for size-dependent separation of liver cells." Biomed Microdevices 9: 637-645.

국문초록

척수 유래 인간 중간엽 줄기세포(hMSC)는 낮은 면역원성과 자가재생 및 다분화능으로 인해 줄기세포치료 원료로서 기대되고 있다. 인간 중간엽 줄기세포는 다양한 크기의 세포군으로 이뤄져 있고, 신속 자가 재생 능력을 가진 RS (rapidly self-renewing) 세포, 섬유아세포(fibroblastic)의 형태를 가진 길쭉한 형태의 SS (spindle-shaped) 세포, 그리고 크고 납작한 형태의 FL (flattened) 세포로 구분할 수 있다. 중간엽 줄기세포의 RS 와 SS 세포군은 FL 세포군보다 더 높은 분화능을 보이며, 각 세포군마다 다른 분화능과 증식능력을 가지기 때문에, 전체 세포 집단에서 특정 크기의 세포군을 분류하는 것은 세포치료를 포함한 줄기세포 연구에서 중요한 과제이다.

본 연구에서는, 분리 효율의 향상을 위하여 미세유체칩 여과에 관성 집중을 결합한 채널 설계를 시도하여 중간엽 줄기세포의 크기별 분리에 적용하였다. 유체 유동에 관해 설정한 모델과 분리하고자 하는 입자의 cut-off 두께에 대한 정확한 계산으로 채널 네트워크를 설계하였고, MEMS 공정에 의해 제작된 PDMS-유리 재질의 칩에는 세포액이 유입되는 주채널, 버퍼용액이 주입되는 측면채널, 그리고 여러 개의 다중분지채널이 존재한다. 여러 개의 분지채널은 합쳐져서 나선형으로 변환되며 세포 입자들은 7 회의 회전을 거쳐 복수의 유출구로 배출되어 크기별로 취합 가능하였다. 아울러 주채널의 말단 부분도 나선형으로 변환되어 복수의 유출구로 배출된 세포 입자들을 크기별로 취합 가능하였다. 궁극적으로 작은 (RS 또는 SS 세포)

세포군과 큰 (FL 세포) 세포군으로의 분리에 성공하였으며, 각각 83%와 98%의 회수율과 99%와 76%의 순도를 확인하였다. 이는 종전의 미세유체칩 여과 방식보다 향상된 결과이다. 따라서, 본 연구에서 시도한 크기별 분리 방식의 줄기세포 연구에 대한 역할이 기대된다.

주요어: 인간 중간엽 줄기세포, 크기별 분리, 관성 집중, 미세유체칩 여과, 채널 설계

학번: 2015-22089